Journal Pre-proof

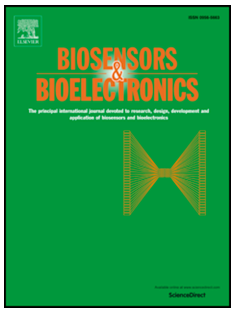

Highly ordered 3D electrochemical DNA biosensor based on dual orientation controlled rolling motor and graftable tetrahedron DNA

Zi Liu, Sheng Lei, Lina Zou, Gaiping Li, Lingling Xu, Baoxian Ye

PII: S0956-5663(19)30838-3

DOI: https://doi.org/10.1016/j.bios.2019.111759

Reference: BIOS 111759

To appear in: *Biosensors and Bioelectronics*

Received Date: 30 August 2019

Accepted Date: 2 October 2019

Please cite this article as: Liu, Z., Lei, S., Zou, L., Li, G., Xu, L., Ye, B., Highly ordered 3D electrochemical DNA biosensor based on dual orientation controlled rolling motor and graftable tetrahedron DNA, *Biosensors and Bioelectronics* (2019), doi: https://doi.org/10.1016/j.bios.2019.111759.

Highly ordered 3D electrochemical DNA biosensor based on dual orientation controlled rolling motor and graftable tetrahedron DNA

Zi Liu, Sheng Lei, Lina Zou, Gaiping Li, Lingling Xu, Baoxian Ye*
College of Chemistry, Zhengzhou University, Zhengzhou 450001, PR China

Abstract

Herein, a robust and highly ordered three-dimensional electrochemical DNA (3D E-DNA) biosensor was proposed, and its orientation was controlled from top down by poly adenine oligonucleotides (polyA-ODNs)-mediated rolling motor (PRM) and graftable tetrahedron DNA (GTD). The GTD with a grafting domain was immobilized on the electrode surface to construct a well-organized sensing interface and controlled the orientation and distribution of the whole system at the "bottom" of this biosensor. The polyA-ODNs regulated the direction and density of the leg DNA attached on PRM at the "top" of the biosensor. The motion was achieved through the target induced cyclic cleaving, which triggered the motor rolling rather than walk. Impressively, the duplex strand DNA (dsDNA) formed after grafting, as a girder, provided a stable support to the soft long single strand (ssDNA), which facilitated the formation of the catalytic center, elevated the efficiency of the rolling cleavage. Under the optimal conditions, the designed biosensor exhibited a lower limit of 0.17 nM and wide linear range from 0.5 nM to 1.5 μM for adenosine rapid detection. Unique dual orientation regulated characteristics of the system increased the probability hybridization enormously and improved the motion efficiency significantly, which offered new avenue of DNA nanomachines development in biosensor platform.

Keywords

Highly ordered, Dual orientation control, 3D electrochemical DNA biosensor, Graftbale tetrahedron DNA, Rolling motor

1. Introduction

Electrochemical DNA (E-DNA) biosensors have offered new opportunities for simple, portable, and sensitive detection of biomolecules associated with clinical diagnosis and monitoring the treatment of diseases (Hsieh et al., 2015; Li et al., 2018a). Usually, the signal generation of these sensors results from a dynamic change, induced by surface hybridization events and redox of reporters labeled on DNA probe, which affects the flexibility of the probe-target complex, giving rise to a significant change in redox peak current (Kang et al., 2016; Liu et al., 2017). Due to the weak conductivity of DNA, signal amplification strategies are always needed to gain more obvious change of peak currents. DNA motor devices including gears (Tian and Mao, 2004; Zhang et al., 2017), walkers (Wang et al., 2011), tweezers (Li et al., 2016), robots (Li et al., 2018b), cranes (Wilner and Willner, 2012), et al, which are based on the accuracy and predictability of Watson-Crick base pairing rules, have gained tremendous attention (Wang et al., 2019b). In addition, it can be propelled by DNAzymes, protein enzymes and strand displacement hold great promises in the area of electrochemical biosensing owing to their cascade signal amplification and highly automated (Peng et al., 2018; Wang et al., 2014). In the infancy of DNA motor establishment, most of the devices perform mechanical locomotion on one-dimensional (1D)

*Corresponding author. *E*-mail address: yebx@zzu.edu.cn (B. X. Ye).

footpath (Ji et al., 2017) or two-dimensional (2D) origami track (Wang et al., 2017). Along with the deepening of the research, the working efficiency of these two type nanomachines is unsatisfactory on account of the low concentration of substrate DNA and the limited work space. Ellington and co-workers proposed the first three-dimensional (3D) DNA motor (Jung et al., 2016), extremely increasing the loading capacity of DNA enrichment due to the large surface to volume ratio of nanoparticle, which opens a new way to better amplification ability.

As a matter of fact, surface chemistry and related surface blocking chemistry must be taken into consideration carefully to improve the sensitivity of the electrochemical biosensors (Chen et al., 2014; Zeng et al., 2017) and the motion efficiency of the nanomotors (Zhang et al., 2018a). The conventional 3D DNA motors established based on the AuNPs cross-link thiolated oligonucleotides through Au-S chemistry, which successfully achieves the random and stepwise movement at nanoscale space (Peng et al., 2017). Unfortunately, very most of them require sealant backfill to modulate the conformation of DNA on the AuNPs, which result in the worse stability of the DNA substrate and low rates of work efficiency, that remains a challenge in designing more stable and high efficiency DNA motors (Chen et al., 2017; Feng et al., 2018). Poly adenine (polyA) has been demonstrated that prefer binds to gold surface with a high adsorption affinity compared to the Au-S chemistry (Opdahl et al., 2007; Schreiner et al., 2010). Besides, backfilling of sealant is not needed any more. The spatial distribution and hybridization ability of the polyA block mediated oligonucleotides assembled on AuNPs (polyA-ODNs-AuNPs) can be regulated precisely through alter the length of the polyA (Pei et al., 2012; Zhu et al., 2015), which makes it a desirable surface modification strategy. We turn our attention to employ it to construct a 3D rolling motor, which not only enrich the DNA substrate strands, but also improve the stability of the rolling motor and control the architecture of it. In addition, the different modified surface influence on the rolling efficiency of the motor is studied, which is not investigated ever.

It is well known that, the sensing interface is vital to the electrochemical biosensor (Lin et al., 2014; Wang et al., 2019a). However, after extensive literature review, the sensing interface, what the motors most worked in is still limited in single strand or origami track, which inevitably involves some drawbacks of collapse and poor controllability (Xu et al., 2019; Yan et al., 2018). Thus, it is hard to regulate the morphology of the sensing surface previously. Tetrahedron DNA with well-defined and rigid architectures can regulate the direction and density of the aptamer on the sensing interface (Liu et al., 2019). It can also avert the nonspecifically absorb and entanglement of the single stranded DNA aptamer, that makes it favorable nanomaterials (Zhou et al., 2017; Zhou et al., 2018). It consists of four single-strand nucleic acids and the longest one contains a specific recognition sequence with the target. We all know that, the longer the DNA strand, the more difficult to synthesize and the higher cost. In practice, for different targets detection, diverse tetrahedron DNA needs to be resynthesized, which causing unnecessary waste of time and raw materials (Dong et al., 2015; Zhang et al., 2018b). On account of these insufficiencies, it is of critical importance to construct a distinctive tetrahedron DNA that is general enough to simultaneously establish different sensing strategy to satisfy the requirements of the vast number of target analytes. .

In this work, a highly ordered and dual orientation controlled 3D electrochemical DNA biosensor is constructed based on polyA mediated rolling motor (PRM) and graftable tetrahedron DNA (GTD). The employment of polyA-ODNs not only abstains from backfilling of sealants but also regulates the density and direction of the substrate DNA attached on the PRM. The GTD is

designed unspecific, which is decorated on the electrode to construct a 3D sensing interface, regulate the distribution of the whole system and control the orientation of the capture probe at the bottom of this biosensor. The recognition sequence is programmed on a DNA bridge probe (DBP) carrying a grafting domain with it. Interestingly, the duplex strand DNA (dsDNA), formed after DBP grafted on GTD, possess an innate advantage in improving sensitivity, which makes the construction of the biosensor however remarkable. It is convenient to establish different sensing strategies simultaneously by simply replace the recognition section of the DBP without resynthesizing the tetrahedron DNA corresponding to the target. Additionally, target induced cyclic cleaving triggered the PRM rolling rather than walk, which provides a new motion mechanism. In summary, the method based on the proposed rolling motor and graftable tetrahedron DNA raised the detection sensitivity and motion efficiency as well as revealed a great potential application in biomarker assay.

2. Experimental section

2.1. Chemicals and Materials

Tris (2-carboxyethyl)-phosphine hydrochloride (TCEP), magnesium chloride hexahydrate ($MgCl_2 \cdot 6H_2O$), sodium perchlorate ($NaClO_4$) were purchased from Sigma−Aldrich (St. Louis, MO). All the DNA oligonucleotides (Table S1 in the Supplement materials) were synthesized and purified by Sangon Biotech Co., Ltd. (Shanghai, China). All solutions were prepared with Milli-Q water (18 MΩ·cm resistivity) from a Millipore system.

TM buffer: 20 mM tris and 50 mM $MgCl_2$, pH 8.0; 10 mM PBS buffer: 10 mM PB, 0.1 M NaCl, pH 7.4; 100 mM PBS buffer: 100 mM PB, 1 M NaCl, pH 7.4; TCEP solution: 100 mM in water.

2.2. Electrochemical detection

Electrochemical measurements were performed on a CHI-650A electrochemical workstation (Chenhua Instruments Co., Shanghai, China). A three-electrode system was made up of a Pt wire as counter electrode, an Ag/AgCl electrode (saturated KCl) as reference electrode and a modified gold electrode (3 mm in diameter) as the working electrode. Cyclic voltammetry (CV) and electrochemical impedance spectroscopy (EIS) measurement were conducted in the PBS containing 0.1 M KCl as supporting electrolyte and 5.0 mM $[Fe(CN)_6]^{3-/4-}$ as redox probe. EIS conditions: initial potential of 5 mV; frequency range from 0.1−100 KHz; amplitude of 5 mV. The differential pulse voltammetry (DPV) responds were obtained in 2 mL PBS (containing 0.1 M $NaClO_4$, pH 7.4). DPV conditions: potential range from 0 V−0.5 V; sample width of 0.03 s; modulation amplitude of 0.05 V; pulse width of 0.05 s.

2.3. Construction of 3D DNA rolling motor

The synthesis of AuNPs with diameter of 13-nm was based on the citrate reduction method (Ambrosi et al., 2007). The polyA-ODNs comprised of a polyA block and a ribonucleobase (rA) cleavage point with ferrocene tagged at the 5'- terminus. The preparation of polyA-ODNs modified AuNPs was according to the protocol by Fan and co-workers (Pei et al., 2012). Briefly, AuNPs was incubated with polyA-ODNs in a ratio of 1:200 for 16 h with gentle shaking. Subsequently, 100 mM PBS (100 mM PB, 1 M NaCl, pH 7.4) was added to the above mixture in a total of five salting steps, and every half an hour between steps, to reach a final concentration of 10 mM (10 mM PB, 0.1 M NaCl, pH 7.4). After that, the salted mixture was allowed to continue incubated for another 40 h at room temperature to further facilitate the formation of polyA-ODNs-AuNPs. The nanoparticles were collected by centrifugation (12000 rmp, 20 min, 4 ℃). After washing three times with 10 mM PBS (10 mM PB, 0.1 mM NaCl, pH 7.4), the

nanoparticles were resuspended in it and put in 4 ℃ for further use.

2.4. Construction of GTD-based aptasensing interface

Each of the four ODNs (A, B, C and D) was treated with 3 mM TCEP for 2 h in the dark to cleave the disulfide linkage. The equal quantities of monomers for formation of GTD were mixed in TM buffer at a final concentration of 1 μM and then heated to 95 ℃ for 5 min and cooled down to room temperature. Gold electrode was firstly immersed in piranha solution (98% H_2SO_4:30% H_2O_2 = 3:1) for about 30 min. After treated with 1, 0.3, 0.05 μm alumina slurry, the polished electrode was then sonicated in ethanol and pure water for 2 min each. Then the electrode was electrochemically cleaned in 0.5 M H_2SO_4 solution by scanning the potential between the oxidation and reduction of gold. Subsequently, GTD was dropped on the cleaned electrode surface immediately, and kept them at 25 ℃ in the dark overnight.

3. Results and discussion

3.1 Design strategy

The operating principle is illustrated in Schemes 1. DNA sequences used in this system are listed in Table S1. The device is composed of a graftable tetrahedron DNA (GTD), a DNA bridge probe (DBP) and a polyA mediated 3D DNA rolling motor (PRM). The GTD with a grafting spire is decorated on the gold electrode surface through Au-S bond. The DBP is designed elaborately, which contains two binding arms, a catalytic center, a programmable recognition region and a grafting domain. The PRM is constructed on a 13 nm – sized AuNPs surface that is coated with diblock-ODNs including a polyA block and a ribonucleobase (rA) cleavage point with ferrocene tagged at the 5'- terminus. Firstly, the DBP is hybridized with GTD through the grafting domain of the both. Subsequently, PRM is captured onto the electrode surface through two asymmetrically binding arms (one is 15 bases length and the other is 7 bases length) and moved autonomously upon the target initiated cleavage of diblock-ODNs abide by burnt-bridge mechanism. When the target exists, the catalytic core of the DBP is activated, and the cleavage triggers the 3D DNA motor rolling with Mg^{2+} cofactors. The short fragment dissociates from the substrates, while the long fragment, in contrast, keeps hybridized with the DBP to avoid the PRM getting lost from the system. Subsequently, the free short fragment of another diblock-ODNs searches for and binds to DBP to accomplish a strand replacement takes place through branch migration, whereby the cleaved substrate fragment is replaced by the intact substrate molecule to form a more stable pseudo continuous DNA duplex. As the target incensement, the current signal gradually decreases. When the target is absence, the catalytic core maintained fallow. In this process, the GTD served as a scaffold to provide a steady support, controlled the density and orientation of the DBP at the "bottom" of the 3D E-DNA sensor. The duplexes DNA formed after DBP grafted on the GTD, as a girder, facilitated the confirmation of the catalytic center augmented the efficiency of the rolling cleavage reaction. The polyA block adjusted the distribution and direction of the diblock-ODNs attached on the AuNPs at the "up" of the 3D E-DNA sensor. It circumvented the backfill of the sealant, improved the hybridization efficiency of the PRM and avoided contamination and uncertainty in displacement. This dual orientation controlled 3D E-DNA biosensor unexceptionable increased the probability of hybridization and the rolling efficiency, further accelerated the development of DNA nanomotors in biosensor platform.

Scheme 1.

3.2. CV and EIS characterization of the biosensor assemble

Cyclic voltammetry (CV) and electrochemical impedance spectroscopy (EIS) were utilized to verify the stepwise fabrication of electrochemical biosensor. Before that, native gel electrophoresis was employed to certify the successful self-assembly of GTD (Figure S1). UV–vis spectra were used to characterize the successful synthesis of 3D rolling motor (Figure S2). As shown in Figure 1A (CV), a pair of well-defined redox peaks from $[Fe(CN)_6]^{3-/4-}$ was observed for bare Au electrode (curve a). Since negatively charged phosphate backbone of DNA was able to repel $[Fe(CN)_6]^{3-/4-}$, the peak current obviously decreased after modification with GTD (curve b). As the DBP was grafted on the sensing surface, the current signal further decreased (curve c). The subsequent incubation of PRM caused a dramatic decrease of redox currents (curve d), because it aggrandized the electrostatic repulsive force of $[Fe(CN)_6]^{3-/4-}$ solution. When target was presence, the catalytic core was activated and cyclic rolling cleavage was happened, which reduced the negative charge of the electrode. Therefore, the intensities of the CV peaks recover to some extents (curve e). The consistent experiment results were revealed by the EIS measurements (Figure 1B). Additionally, the AFM was used to character the modification electrode (Figure S3). The results further revealed the successful construction of the 3D E-DNA biosensor.

Figure 1.

3.3. Condition optimization

In order to optimize the detection conditions for improving the velocity and sensitivity of the biosensor, the length of polyA block (A5, A10, A15 A20 and A25), the graft time and the rolling time were studied by DPV in PBS (10 mM PB, 0.1 M NaCl, 0.1 M KCl, 0.1 M $NaClO_4$, pH 7.4). Previous studies have already demonstrated that the hybridization efficiency increases with increasing polyA length (Pei et al., 2012; Zhu et al., 2015). Herein, the impact of polyA length on the rolling efficiency was investigated. As illustrated in Figure 2A, the rolling efficiency was obviously improved from polyA5 to polyA15 and gradually decreased from polyA15 to polyA25. These results demonstrated that the increased inter-strand spacing effectively decreased the space steric hindrance and elevated the rolling efficiency of dual orientation controlled 3D DNA rolling nanomachine. The cleavage efficiency reached maximum at polyA15 (~93.1%). Thus, the polyA15 was chosen in the following experiment. The decreased rolling efficiency of polyA20 and polyA25 was probably due to the long spacing of substrate blocks hindered the movement of DNAzyme walkers. The electrochemical signal originates from the ferrocene modified on the di-block DNA, which decorated on the AuNPs. Therefore, the graft time has significant influence on the peak current and need to be investigated. As shown in Figure 2B, the incubation time from 10 to 60 min led the current signal increasing, and the maximum platform could be observed after 50 min. Hence, 50 min was selected as the optimum graft time. For speedy detection, the rolling time of Mg^{2+}-driven dual orientation controlled 3D DNA nanomachine was the decisive factor. As seen from Figure 2C, the current decreased from 20 min to 60 min and kept stable after 60 min, which suggested that 60 min for rolling was enough to achieve the highest electrochemical responses.

Figure 2.

3.4. Comparison of different sensing strategy

In order to more intuitively confirm rolling efficiency and moving velocity, the electrochemical signal comparison was performed between a holistic tetrahedron DNA based sensors (HTDS) and graftable tetrahedron DNA based sensors (GTDS). The HTD itself was specific and the recognition sequence was programmed in the longest strand of it; while the GTD was unspecific, and whose recognition sequence was designed in the DBP grafted on it. As illustrated in Figure S4, in the absence of the target, the peak current of GTDS was almost 2 times higher than HDPS under the same graft time. In the presence of the target (150 nM), the cleavage capacity of the catalytic core was activated. Under the same conditions, the current change indicated that the rolling efficiency of GTDS (57%) obviously elevated than HTDS (32%). This result indicated that the dual orientation controlled 3D E-DNA biosensor based on GTD exhibited superior performance in terms of both grafting time and rolling efficiency. That is presumably due to the rigid dsDNA formed at the spire of GTD supported the soft long ssDNA and the conformation of catalytic core, which facilitated the hybridization reaction and DNAzyme cleavage.

3.5. Performance of the 3D electrochemical DNA biosensor

Adenosine was used as the model analyte to exploring the application of this proposed 3D E-DNA biosensor under the optimal experimental conditions. As shown in Figure 3A, the DPV response decreased with the increase of adenosine concentrations. The more targets were introduced in this system, the more catalytic cores were activated, which triggered cyclic rolling cleave reaction and resulted in the signal probe cleaved. A decrease of peak current was observed. The Figure 3B demonstrated a well linear relation between the peak currents and the logarithm of adenosine concentrations from 0.5 nM to 1500 nM. The regression equation is $I_p = -0.26\ \lg C + 1.07$ with a correlation coefficient of 0.9975, where I_p and C represent the current intensity and the concentration. The detection limit was 0.17 nM corresponding to the signal of blank plus 3 times the SD (standard deviation). In addition, Table 1 depicted that the proposed method expressed a wider linear range and a lower detection limit. From comparison to previous methods for adenosine detection demonstrates an outstanding analytical performance of the 3D E-DNA biosensor.

Figure 3.

Table 1.

3.6. Selectivity, stability and reproducibility of the 3D electrochemical DNA biosensor

To investigate the specificity of the proposed 3D E-DNA biosensor, nucleoside family (Figure 4) and other interferents exhibited in the practical sample (Figure S5) were chosen as the potential rivals to this biosensor. As illustrated in Figure 4A and Figure S5, no significant change in current response was found in the absence of the target substances, while there was an obviously change about current signal even with 10-fold lower target adenine (150 nM). In addition, when targets were mixed with the aforementioned different interfering substances, the current response was almost the same as the value obtain from adenine only. The results demonstrated the proposed 3D DNA electrochemical biosensor has satisfactory selectivity and potential usability. The stability of the 3D E-DNA biosensor was also monitored by storing it at 4 ℃ and measured every 2 days. After 16 days, the biosensor retained 86% of its original response. Even 20 days later, the current

value of the biosensor still kept at 80% of its initial value (Figure 4B), which suggested that the proposed biosensor had good performance in stability. Moreover, the reproducibility was studied by employing twelve repetitive measurements of the target under the same condition, and the RSDs (relative standard deviations) was 3.91%, indicated that the reproducibility of the proposed aptasensor was approving.

Figure 4.

3.7. Universality study of graftable tetrahedral DNA

In order to verify the universality of the GTD, the same batch synthesized GTD was employed to analysis CEA using double aptamer recognized (DAR) strategy, the details principle was illustrated as Scheme S1. Briefly, one aptamer of the CEA was arranged in a new DBP (CEA-DBP) grafted on the GTD, and another one was acted as signal probes with ferrocene tagged at the 5'-terminus. In the presence of the CEA, the signal probe was captured on the electrode to convert the concentration of target to electrochemical signal. Under the optimal conditions (Figure S6), different concentration of CEA was detected to verify the ability of the DAR biosensor. As presented in Figure S7A, the peak currents rose up significantly as the sensor was titrated with increasing amounts of target from 0.01 pM to 5 nM. The Figure S7B displayed a well linear relationship between peak currents and logarithm of CEA concentrations following the linear equation of $I_p = 0.1\ lgC_{CEA} + 0.62$ with a squared correlation coefficient R^2 of 99.4%. The detection limit of CEA was calculated to be 3.33 fg/mL. The result indicated that the same batch synthesized GTD was general enough satisfying to develop of different biosensor strategy for target analysis，and it was convenience and time saving.

3.8. Applicability of the Proposed Biosensor in Real Sample Analysis

In order to assess the effectiveness of the dual orientation controlled 3D E-DNA biosensor in clinical application, recovery experiments were performed in PBS buffer using10-fold diluted human serum sample (obtained from the First Affiliated Hospital of Zhengzhou University, China). To begin with, no adenine was found in human serum. After that, six different concentrations of adenosine were added into the diluted human serum, and were then tested using the proposed biosensor. The obtained recoveries in the range of 96.66% to 110.7% were listed in Table S2, and the RSD values were from 3.1% to 5.7%. This result suggested that the proposed 3D E-DNA biosensor could assay adenine in real serum samples with satisfactory reliability and exhibited potential applications in clinical diagnostics.

Additionally, the CEA analysis experiment was also performed in real samples. Five patient serum samples (obtained from the First Affiliated Hospital of Zhengzhou University, China) were measured using the mentioned double aptamer recognized strategy and each sample was test three times. The patient samples were 10-fold diluted in the procedure of the experiment to make it in the liner range of this strategy. The results were listed in Table S3, which were consisted with the electrochemiluminescence (ECL) method adopted by hospital. As can be seen from the Table S3, RSD of the five different concentration of CEA was -2.94%, 4.48%, 3.25%, -5.14%, and -2.1%, respectively. The data suggested that the proposed GTD-based double aptamer recognition aptasensor was applicable and feasible for applications in the biological samples, and the GTD designed in this work was practical.

4. Conclusion

In this study, we developed a highly ordered three-dimensional electrochemical DNA (3D E-DNA) biosensor integrating a poly adenine mediate rolling motor (PRM), DNA bridge probe (DBP) and graftable tetrahedron DNA (GTD). The polyA block attached on the PRM enhanced the anchoring function and effectively prevented nonspecific Au-DNA binding as well as made the substrate adopts an upright conformation that promoted the motion efficiency compared with conventional motors. The 3D sensing interface constructed based on GTD avoided the tangles and collapse of the single strand, which effectively reduced background interference and elevated the detection sensitivity. In addition, the versatility and modularity of DBP facilitated the conformation of the catalytic center, which adds one more force to the improvement of the motion efficiency. Finally, the indirect binding of the sensing surface to the analyte made this approach readily adaptable for analysis of any targets by simple replace the recognition section of the DBP without resynthesizing the tetrahedron DNA corresponding to the target, which provided convenience for biosensor construction. This described 3D E-DNA biosensor with well-organized orientation and distribution from top down shows great potential in development of new devices of DNA nanomotors for biological applications and clinical therapeutics.

Acknowledgments

The authors are sincerely grateful for the financial support from the National Natural Science Foundation of China (No. 21575130).

References

Ambrosi, A., Castaneda, M.T., Killard, A.J., Smyth, M.R., Alegret, S., Merkoci, A., 2007. Anal. Chem. 79, 5232-5240.

Cai, S., Sun, Y.H., Lau, C.W., Lu, J.Z., 2013. Anal. Chim. Acta 761, 137-142.

Chen, J.B., Zuehlke, A., Deng, B., Peng, H.Y., Hou, X.D., Zhang, H.Q., 2017. Anal. Chem. 89, 12888-12895.

Chen, X.Q., Zhou, G.B., Song, P., Wang, J.J., Gao, J.M., Lu, J.X., Fan, C.H., Zuo, X.L., 2014. Anal. Chem. 86, 7337-7342.

Dong, S.B., Zhao, R.T., Zhu, J.G., Lu, X., Li, Y., Qiu, S.F., Jia, L.L., Jiao, X., Song, S.P., Fan, C.H., Hao, R.Z., Song, H.B., 2015. ACS Appl. Mater. Interfaces 7, 8834-8842.

Feng, C., Wang, Z.H., Chen, T.S., Chen, X.X., Mao, D.S., Zhao, J., Li, G.X., 2018. Anal. Chem. 90, 2810-2815.

Hsieh, K., Ferguson, B.S., Eisenstein, M., Plaxco, K.W., Soh, H.T., 2015. Acc. Chem. Res. 48, 911-920.

Ji, Y.H., Zhang, L., Zhu, L.Y., Lei, J.P., Wu, J., Ju, H.X., 2017. Biosens. Bioelectron. 96, 201-205.

Jung, C., Allen, P.B., Ellington, A.D., 2016. Nat. Nanotechnol. 11, 157-163.

Kang, D., Ricci, F., White, R.J., Plaxco, K.W., 2016. Anal. Chem. 88, 10452-10458.

Li, C., Hu, X.L., Lu, J.Y., Mao, X.X., Xiang, Y., Shu, Y.Q., Li, G.X., 2018a. Chem. Sci. 9, 979-984.

Li, D.D., Cheng, W., Li, Y.J., Xu, Y.J., Li, X.M., Yin, Y.B., Ju, H.X., Ding, S.J., 2016. Anal. Chem. 88, 7500-7506.

Li, S.P., Jiang, Q., Liu, S.L., Zhang, Y.L., Tian, Y.H., Song, C., Wang, J., Zou, Y.G., Anderson, G.J., Han, J.Y., Chang, Y., Liu, Y., Zhang, C., Chen, L., Zhou, G.B., Nie, G.J., Yan, H., Ding, B.Q., Zhao, Y.L., 2018b. Nat. Biotechnol. 36, 258-264.

Lin, M.H., Wen, Y.L., Li, L.Y., Pei, H., Liu, G., Song, H.Y., Zuo, X.L., Fan, C.H., Huang, Q., 2014. Anal. Chem. 86, 2285-2288.

Liu, J.Q., He, D.G., Liu, Q.Q., He, X.X., Wang, K.M., Yang, X., Shangguan, J.F., Tang, J.L., Mao, Y.F., 2016a. Anal. Chem. 88, 11707-11713.

Liu, X.P., Yan, Z.Q., Sun, Y.H., Ren, J.S., Qu, X.G., 2017. Chem. Commun. 53, 6215-6218.

Liu, Y.X., Ma, H.M., Zhang, Y., Pang, X.H., Fan, D.W., Wu, D., Wei, Q., 2016b. Biosens. Bioelectron. 86, 439-445.

Liu, Z., Lei, S., Zou, L.N., Li, G.P., Xu, L.L., Ye, B.X., 2019. Biosens. Bioelectron. 131, 113-118.

Opdahl, A., Petrovykh, D.Y., Kimura-Suda, H., Tarlov, M.J., Whitman, L.J., 2007. Proc. Natl. Acad. of Sci. U. S. A. 104, 9-14.

Pei, H., Li, F., Wan, Y., Wei, M., Liu, H.J., Su, Y., Chen, N., Huang, Q., Fan, C.H., 2012. J. Am. Chem. Soc. 134, 11876-11879.

Peng, H., Li, X.F., Zhang, H., Le, X.C., 2017. Nat. Commun. 8, 14378.

Peng, H., Newbigging, A.M., Wang, Z., Tao, J., Deng, W., Le, X.C., Zhang, H., 2018. Anal. Chem. 90, 190-207.

Schreiner, S.M., Shudy, D.F., Hatch, A.L., Opdahl, A., Whitman, L.J., Petrovykh, D.Y., 2010. Anal. Chem. 82, 2803-2810.

Sun, J., Jiang, W., Zhu, J., Li, W., Wang, L., 2015. Biosens. Bioelectron. 70, 15-20.

Song, Y.Y, Tang, T., Wang, X., Xu, G.H., Wei, F.D., Wu, Y.Z., Song, Q., Ma, Y.J., Ma, Y.J., Ma, Y.S., Cen, Y., Hu, Q., 2017. Sens. Actuators B: Chem. 247, 305–311.

Tian, Y., Mao, C.D., 2004. J. Am. Chem.Soc. 126, 11410-11411.

Wang, D., Chai, Y.Q., Yuan, Y.L., Yuan, R., 2019a. Anal. Chem. 91, 3561-3566.

Wang, D.F., Vietz, C., Schroder, T., Acuna, G., Lalkens, B., Tinnefeld, P., 2017. Nano lett. 17, 5368-5374.

Wang, F., Lu, C.H., Willner, I., 2014. Chem. Rev. 114, 2881-2941.

Wang, J., Wang, D.X., Tang, A.N., Kong, D.M., 2019b. Anal. Chem. 91, 5244-5251.

Wang, Z.G., Elbaz, J., Willner, I., 2011. Nano lett. 11, 304-309.

Wilner, O.I., Willner, I., 2012. Chem. Rev. 112, 2528-2556.

Xu, Z.Q., Chang, Y.Y., Chai, Y.Q., Wang, H.J., Yuan, R., 2019. Anal. Chem. 91, 4883-4888.

Xu, L., Shen, X., Li, B.Z., Zhu, C.H., Zhou, X.M., 2017. Anal. Chim. Acta 980, 58-64.

Yan, T., Zhu, L., Ju, H., Lei, J., 2018. Anal. Chem. 90, 14493-14499.

Yang, K., Wang, H.Z., Ma, N., Zeng, M., Luo, H.Q., He, D.G., 2018. ACS Appl. Mater. Interfaces 10, 44546-44553.

You, J.H., You, Z.Y., Xu X., Ji, J.G., Lu, T., Xia, Y.H., Wang, L.P., Zhang, L.Y., Du, S.H., 2019. Microchimica Acta 186, 43-50.

Zeng, D.D., Wang, Z.H., Meng, Z.Q., Wang, P., San, L.L., Wang, W., Aldalbahi, A., Li, L., Shen, J., Mi, X.Q., 2017. ACS Appl. Mater. Interfaces 9, 24118-24125.

Zhang, P., Jiang, J., Yuan, R., Zhuo, Y., Chai, Y.Q., 2018a. J. Am. Chem. Soc. 140, 9361-9364.

Zhang, P., Lin, Z.F., Zhuo, Y., Yuan, R., Chai, Y.Q., 2017. Anal. Chem. 89, 1338-1345.

Zhang, Y., Shuai, Z.H., Zhou, H., Luo, Z.M., Liu, B., Zhang, Y.N., Zhang, L., Chen, S.F., Chao, J., Weng, L.X., Fan, Q.L., Fan, C.H., Huang, W., Wang, L.H., 2018b. J. Am. Chem. Soc.140, 3988-3993.

Zhang, X.R., Zhao, Y.Q., Li, S.G., Zhang, S.S., 2010. Chem. Commun. 46, 9173-9175.

Zhou, X.Y., Zhao, M., Duan, X.L., Guo, B., Cheng, W., Ding, S.J., Ju, H.X., 2017. ACS App. Mater. Interfaces 9, 40087-40093.

Zhou, Y., Wang, H.J., Zhang, H., Chai, Y.Q., Yuan, R., 2018. Anal. Chem. 90, 3543-3549.

Zhu, Y., Jiang, X.X., Wang, H.Y., Wang, S.Y., Wang, H., Sun, B., Su, Y.Y., He, Y., 2015. Anal. Chem. 87, 6631-6638.

Table 1. Analytical performances of different methods for adenosine detection.

Methods	Dynamic range	Detection limit	references
Fluorescence	1μM - 100 μM	420 nM	(Sun et al., 2015)
Fluorescence	0.33 nM - 167μM	0.22 nM	(Song et al., 2017)
Fluorescence	0 nM - 320 μM	2.4 nM	(You et al., 2019)
Chemiluminescence	1 nM -10 μM	0.5 nM	(Cai et al., 2013)
Photoelectrochemical	0.1 nM - 1μM	3.2 nM	(Zhang et al., 2010)
Photoelectrochemical	0.3 nM - 0.2 μM	0.1 nM	(Liu et al., 2016b)
Electrochemiluminescence	1 nM -10 μM	0.75 nM	(Liu et al., 2016a)
Colorimetric sensor	50 Nm - 6μM	17 nM	(Xu et al., 2017)
DNAzyme walker-based sensor	10 nM - 3.2 μM	3.33 nM	(Yang et al., 2018)
DNA rolling motor based sensor	0.5 nM - 1.5 μM	0.17nM	This work

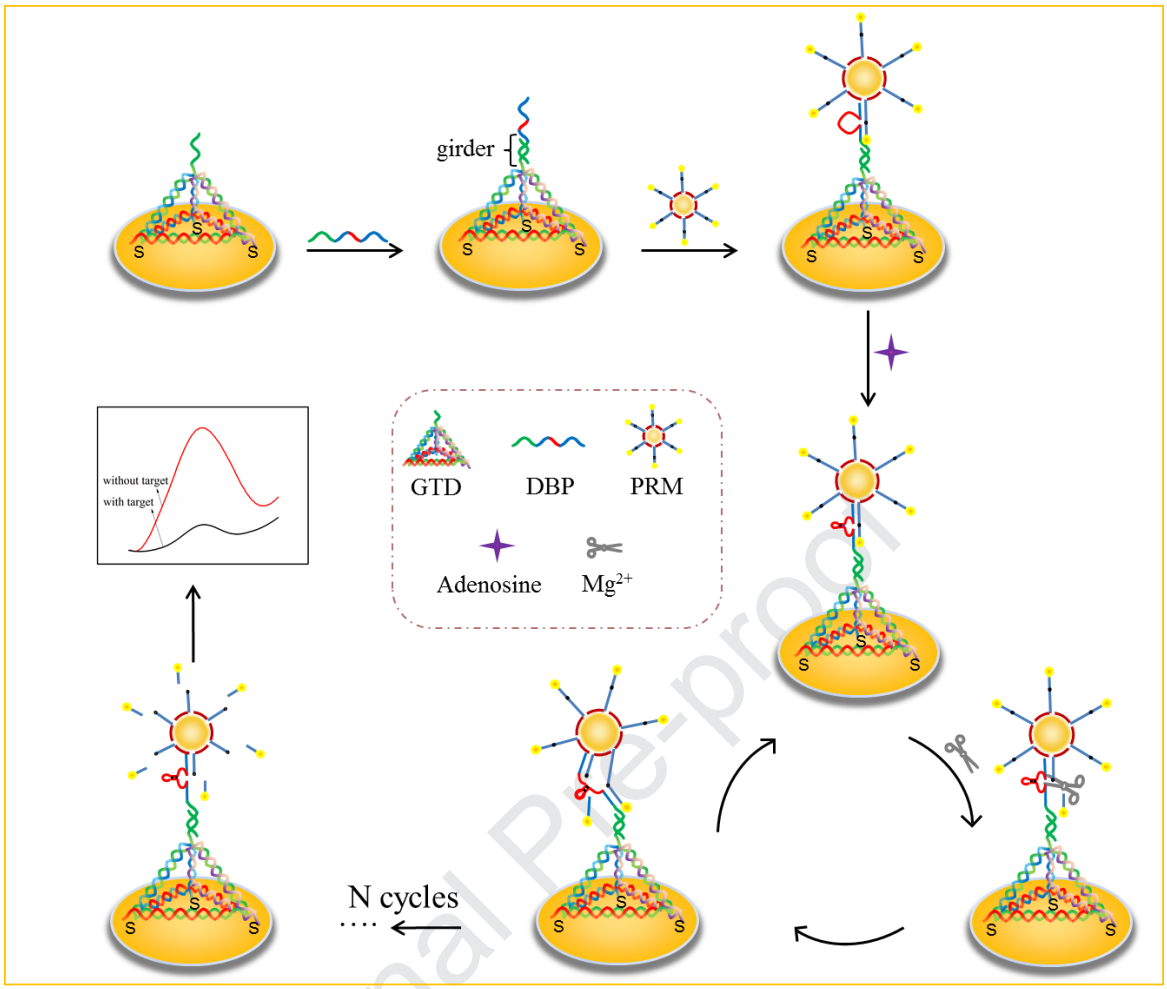

Scheme 1. Schematic illustration of the dual orientation controlled 3D electrochemical DNA biosensor.

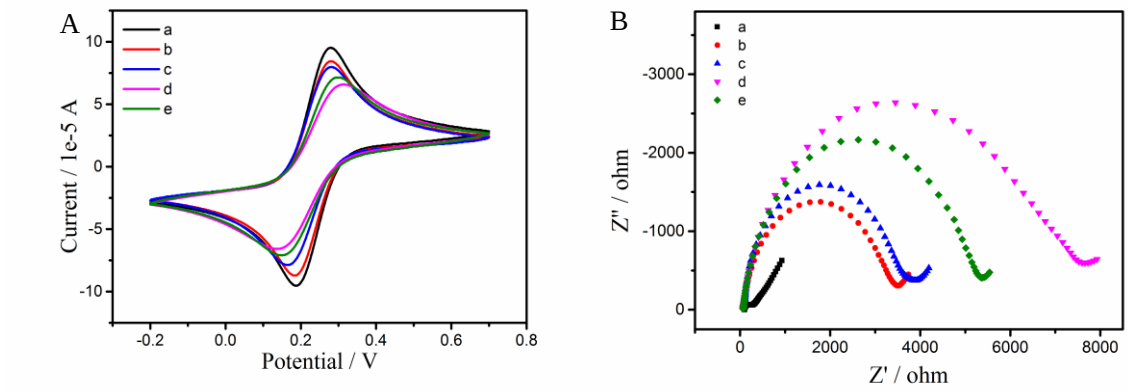

Figure 1. (A) Typical CV responses and (B) EIS diagram responses of different modified electrodes: (a) bare Au, (b) GTD/bare Au, (c) DBP/GTD/bare Au, (d) PRM /DBP/GTD/bare Au, (e) adenosine and Mg^{2+}/PRM /DBP/GTD/bare Au.

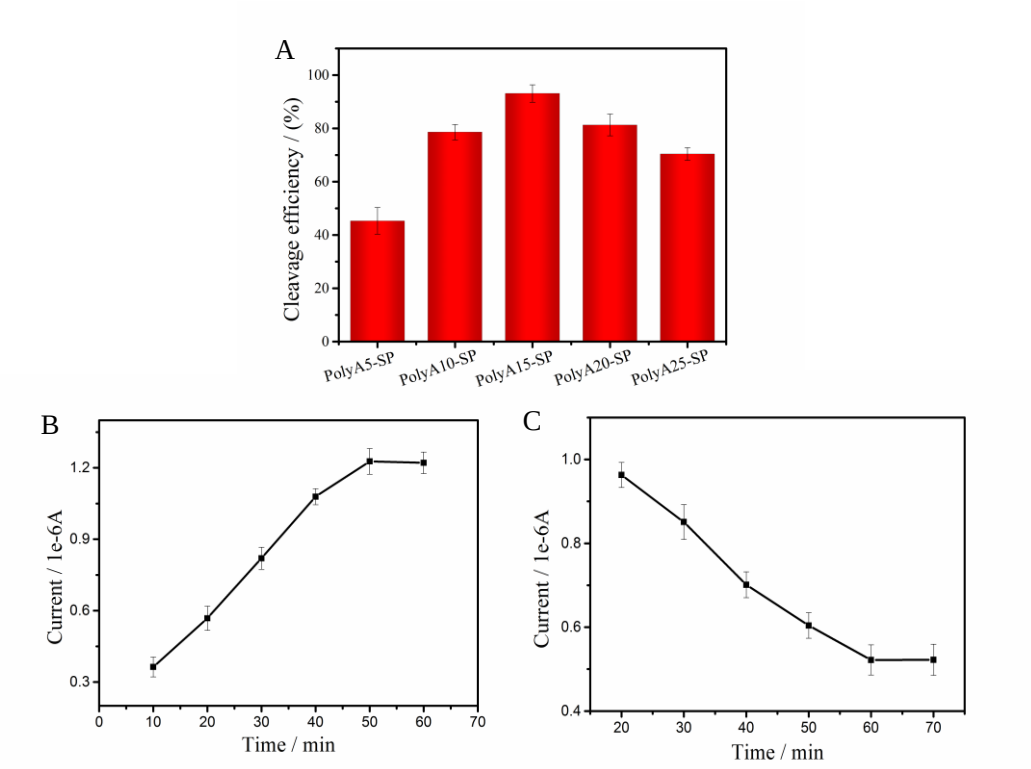

Figure 2. (A) Rolling efficiency of the different polyA-ODNs triggered by target. (B) Grafting time of the PRM. (C) Rolling time of the 3D E-DNA machine in the presence of 20 mM Mg^{2+}.

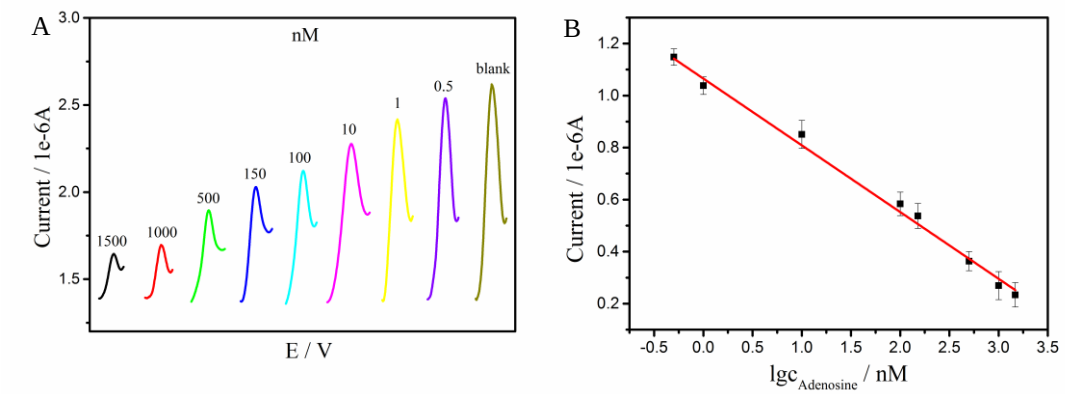

Figure 3. (A) DPV current responses of the 3D E-DNA biosensors to different concentrations of adenosine. (B) Corresponding calibration plot of the current intensity versus the logarithm of adenosine concentration. (Error bars, SD; n = 3)

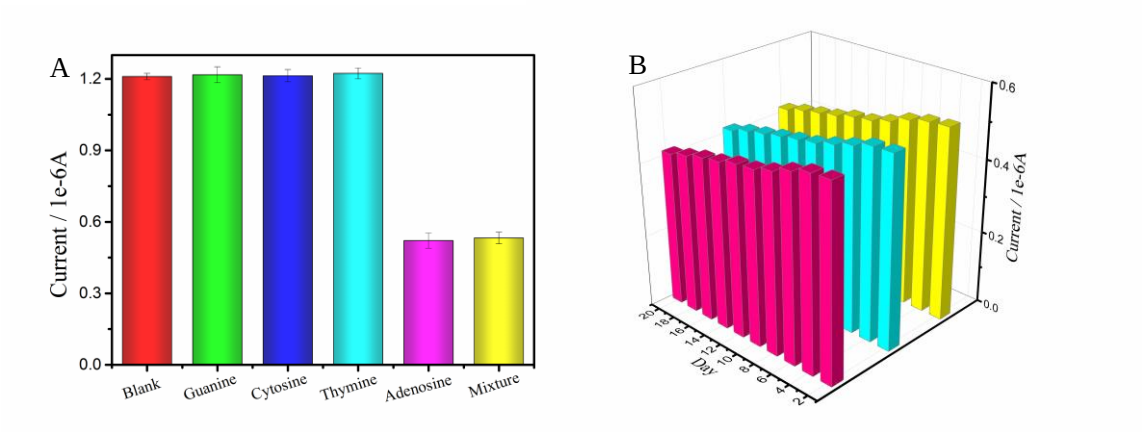

Figure 4. (A) Selectivity of the 3D E-DNA biosensor toward adenosine detection (blank, 1500 nM guanine, 1500 nM cytosine, 1500 nM thymine, 150 nM adenosine, and a mixture of them). (B) Stability of the 3D E-DNA biosensor with 150 nM adenosine. (Error bars: SD, n = 3)

Highlights:

· The 3D electrochemical DNA biosensor is highly ordered with the density and orientation of its component are well controlled from top down.

· The rolling motor is well-designed and triggered rolling by target induced cyclic cleaving.

· A distinctive graftable tetrahedron DNA is proposed to constructed 3D sensing surface regulated the density of the whole system.

· The graftable tetrahedron can be used to simultaneously construct different sensing strategies without re-synthesizing according to the target.

· Poly adenine prompts the substrate DNA of rolling motor adopts an upright conformation and programs the direction and density of substrate DNA precisely.

Declaration of interests

☑The authors declare that they have no known competing financial interests or personal relationships that could have appeared to influence the work reported in this paper.

☐The authors declare the following financial interests/personal relationships which may be considered as potential competing interests: